Available online at www.sciencedirect.com
SCIENCE DIRECT®
Journal of Magnetic Resonance 181 (2006) 271–279
JMR Journal of Magnetic Resonance
www.elsevier.com/locate/jmr

Centric-scan SPRITE magnetic resonance imaging with prepared magnetisation

Alexandre A. Khrapitchev, Benedict Newling, Bruce J. Balcom *

Department of Physics, University of New Brunswick, P.O. Box 4400, Fredericton, NB, Canada E3B 5A3

Received 30 September 2005; revised 18 May 2006
Available online 12 June 2006

Abstract

The combination of contrast preparation with centric-scan SPRITE imaging readout is investigated. The main benefit of SPRITE, its ability to image objects with short T_2, is retained. We demonstrate T_1 and T_2 mapping as examples of magnetisation preparation followed by magnetisation storage and spatially resolved encoding. A strategy for selection of the most advantageous imaging parameters for contrast mapping is presented.

Keywords: MRI, short T_2^*; SPRITE; Magnetisation preparation; Contrast imaging; Pure phase encoding; Single point imaging

1. Introduction

Single-point imaging (SPI) is a well-established tool for studies of systems with short MRI signal lifetimes, governed by the time constant T_2. These short lifetimes are typical of solids, semi-solids, liquid crystals, confined liquids and many gases. In conventional MRI, the time evolution of magnetisation is measured in the presence of a constant magnetic field gradient (frequency encoding); therefore the lifetime of the MRI signal is a crucial parameter. In contrast, SPI is a purely phase-encoded technique, and magnetisation is sampled at fixed intervals (t_p) after radio frequency (*RF*) excitation, also in the presence of a constant magnetic field gradient. Only one point of *k*-space is sampled for each *RF* excitation, but the magnetic field gradient is changed in steps between consecutive excitations. The magnetisation spends a significantly shorter time in the transverse plane (orthogonal to the polarising magnetic field) than in the frequency encoding case. The possibility of using a relatively short t_p makes SPI well-suited to the imaging of objects with $T_2 < 1$ ms.

The most generally applicable SPI MRI method is SPRITE (Single Point Ramped Imaging with T_1 Enhancement) [1]. One of the principal adaptations of SPRITE employs continuously ramped gradients with data acquisition commencing at the centre of *k*-space (centric-scan SPRITE) [2]. This approach improves the Signal to Noise (S/N) ratio per unit acquisition time, simplifies the image contrast and reduces the gradient duty cycle limitation of previous implementations. SPRITE methods are mostly targeted towards samples with short lifetimes, but they can also be successfully applied in investigations where lifetimes are not a limiting factor.

Image resolution in centric-scan SPRITE is governed by gradient strength, and t_p, whereas blurring is governed by the balance of T_1, α, the rotation angle of magnetisation under the action of *RF* (tip angle) and *TR* (repetition time between pulses) [3]. In some SPRITE cases, in order to obtain homogeneous excitation of the spin system, the duration of the *RF*-pulses is also limited by the maximum spectral width of the object ($G_{\max} \times$ length of the sample). Therefore, extensive signal averaging may be required to achieve a practical S/N ratio (by which we mean sufficient to resolve the necessary detail in the problem at hand). For samples with short T_1, the accumulations can be rapid. For materials with long T_1 any requirement for intensive signal

* Corresponding author. Fax: +1 506 453 4581.
E-mail address: bjb@unb.ca (B.J. Balcom).

1090-7807/$ - see front matter © 2006 Elsevier Inc. All rights reserved.
doi:10.1016/j.jmr.2006.05.012

averaging will lead to a significant increase in experimental time. We note that the collection of multiple FID data points provides a separate, time-efficient route to signal averaging, in some favorable circumstances [3].

Perhaps the greatest attraction of MRI as an imaging modality lies in the flexibility of contrasts which may be imposed upon the image. A careful selection of imaging method can result in quantitative maps of temperature, pH, velocity, diffusion, chemical activity, or one of many other important properties of materials. Serious care must be taken in order to avoid superposition of additional weighting due to temporal signal evolution upon the desired contrast. The ease with which relaxation time contrast may be minimised, makes SPRITE an intuitively appealing MRI technique for a broad range of mapping applications.

One possible way to apply a contrast to an MR image is by ''preparation'' of the magnetisation. At the beginning of a measurement the magnetisation undergoes a sequence of *RF* and gradient pulses according to the desired contrast. The ''prepared'' magnetisation is then stored along the z direction of the polarising magnetic field (the z or *longitudinal* axis) and spoiling gradient pulses are applied to destroy remaining magnetisation in the transverse plane. Thereafter an imaging technique with small tip angle excitations (such as SPRITE, in this case) can be applied in order to spatially resolve the contrast. However, during the readout of k-space the magnetisation will evolve towards a dynamic equilibrium [3], which bears no relation to the preparation and introduces contrast related artefacts in the final map. The sample T_1 is once again a critical parameter as it governs the rate at which dynamic equilibrium develops.

In this paper, we outline the use of centric-scan SPRITE imaging in conjunction with longitudinal magnetisation preparation. This technique provides several natural advantages, but the most valuable is robust imaging contrast. The important features are demonstrated through examples of T_1 and T_2 weighted images of a doped gel phantom. Typical problems of magnetisation preparation imaging, such as edge enhancement and contrast blurring, are discussed separately. A set of general guidelines for the most appropriate choice of readout scheme, for given sample lifetimes, is systematically refined and a strategy for the most advantageous selection of the imaging parameters is presented in conclusion.

2. Theory

There are two common ways to perform contrast weighted imaging by magnetisation preparation. The first is to apply a spin–echo imaging sequence after the magnetisation has been prepared. This is a typical utilisation of preparation combined with the RARE (Rapid Acquisition with Relaxation Enhancement) imaging readout [4]. In this case, the lifetime of the prepared magnetisation will be determined by the spin–spin relaxation mechanism and, therefore, governed by T_2 or even T_2^* in the EPI (Echo-Planar Imaging) case [5]. The second scenario is to store the prepared magnetisation along the longitudinal direction and apply a small angle excitation technique for the spatial encoding. In this case the magnetisation evolution will be determined by the spin–lattice mechanism and is therefore, governed by T_1. Since SPRITE employs a train of small angle excitation *RF*-pulses, in this paper, we will describe only the latter approach. It should also be noticed that a similar methodology can be applied to the FLASH (Fast Low-Angle SHot) imaging technique [6], which utilises the same readout mechanism [7].

2.1. Magnetisation evolution

The original SPRITE technique is a longitudinal steady-state imaging method [1]. The longitudinal magnetisation is driven towards a dynamic equilibrium by applying a series of low tip angle *RF*-pulses (Fig. 1). A dynamic equilibrium is reached when the competing reduction and recovery of the magnetisation reach a balance, and the longitudinal magnetisation has the same amplitude before each *RF* excitation. The equilibrium magnetisation is described as follows:

$$M_\infty = M_0 \frac{1 - \mathrm{e}^{-TR/T_1}}{1 - \cos\alpha \mathrm{e}^{-TR/T_1}}, \tag{1}$$

where α is the *RF*-pulse tip angle; TR, time between *RF*-pulses.

The observed signal intensity at any point is related to the equilibrium longitudinal magnetisation and after the nth *RF*-pulse, M_n is given by

$$M_n = (M_0 - M_\infty)(\cos\alpha \mathrm{e}^{-TR/T_1})^n + M_\infty. \tag{2}$$

The first term depends on n and governs image blurring. The detailed investigation of this particular aspect of SPRITE can be found in [8,9]. The approach to steady state through application of multiple *RF*-pulses has been described in [10].

2.2. Magnetisation preparation

The generalised idea of the magnetisation preparation is depicted in Fig. 2. The ''Preparation'' part consists of all necessary magnetisation manipulations plus its storage

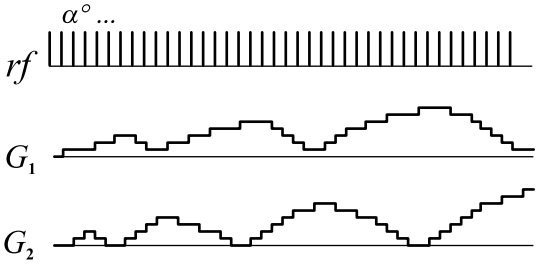

Fig. 1. Single Point Ramped Imaging with T_1 enhancement (SPRITE) sequence.

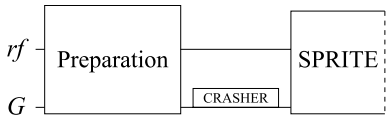

Fig. 2. The magnetisation preparation with an imaging readout sequence.

along the longitudinal direction, "Crusher" is a gradient pulse in all three orthogonal directions, designed to destroy the remaining transverse magnetisation and "Imaging" is a combination of *RF* and gradient pulses for spatial encoding of the prepared magnetisation.

In the case, when the longitudinal magnetisation is reduced from its equilibrium state M_0 by the use of a preparation sequence Eq. (2) can be rewritten as following:

$$M_n = M_i^n + (1 - (\cos\alpha e^{-TR/T_1})^n)M_\infty, \tag{3}$$

where M_i is the initial amplitude of the total magnetisation, and again two terms can be separated. The first term, which depends on M_i and n, governs T_1-mediated blurring of contrast maps. The second term represents recovery of "unprepared" magnetisation towards the steady state, and does not contain the contrast information. However, due to its dominance at the outskirts of k-space, it has an "edge enhancement" effect on some contrast weighted images and, therefore, on the final maps. The time evolution of these two terms is demonstrated in Fig. 3a, where the prepared magnetisation is denoted as M_P (the first term in Eq. (3)), unprepared as M_U (the second term in Eq. (3)), and the sum of these two components as M_T.

The edge enhancement can be eliminated by phase cycling of the storage *RF*-pulse. If the prepared magnetisation is stored along the negative directions of the z-axis (Fig. 3b), then the contrast dependant term has an opposite

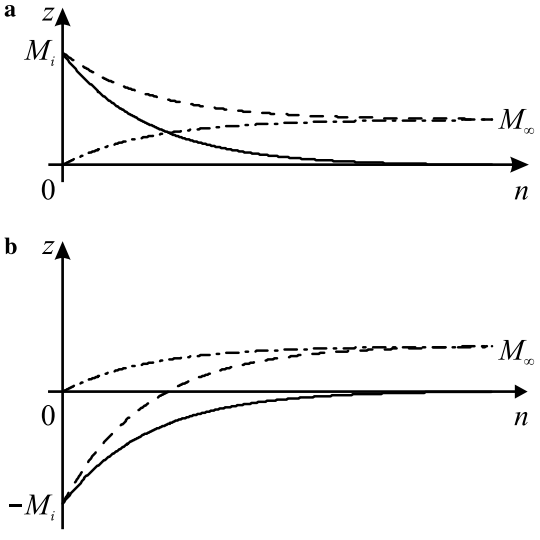

Fig. 3. The magnetisation evolution during a centric-scan SPRITE readout. The magnetisation is stored along the (a) positive and (b) negative directions of the z-axis. Where M_P (—) is the transient (prepared) component and M_U (–·) the steady state (unprepared) component of M_T (– –) which is the total magnetisation, which has an initial and final amplitude $M_T(0) = \pm M_i$ and $M_T(\infty) = M_\infty$, respectively.

sign, but the steady-state term remains the same. Therefore, it can be removed by summation of the positively and negatively stored magnetisation (Figs. 3a and b) with an appropriate shift of the acquisition phase.

The next step is to maintain the desired resolution by controlling the level of blurring. Contrast blurring (by which we mean loss of resolution in an image derived entirely from the prepared magnetisation after phase cycling) can be significantly reduced by keeping the magnetisation time-evolution curve above a certain level. An intuitively appealing rule of thumb for the threshold magnetisation level is e times lower than the initial value, $M(N) = M_i/e$. This choice will be justified by the discussion that follows. The minimum TR/T_1 ratio is naturally determined by hardware limitations, in particular the minimum time required for completion of gradient switching. Decreasing α will reduce blurring only at the cost of a reduction in S/N. The only satisfactory way to reduce blurring is by the segmentation of k-space and the introduction of multi-leaf trajectories (each leaf being one locus in k-space, several of which are assembled to form the whole k-space raster), a strategy which is described in detail in [2]. The necessary number of leaves in a SPRITE sequence can be determined from:

$$(\cos\alpha \cdot e^{-TR/T_1})^N > e^{-1}, \tag{4}$$

where N, is the maximum number of points in each leaf. And therefore N should be

$$N < \frac{1}{TR/T_1 - \ln(\cos\alpha)}. \tag{5}$$

There are three important instances of this equation. The first case, when α is small and $\ln(\cos\alpha)$ can be neglected, causes Eq. (5) to evolve into:

$$N < \frac{T_1}{TR}, \tag{6}$$

and, since $N \cdot TR$ is the maximum leaf-length, the important equation is

$$\text{Leaf-length} < T_1. \tag{7}$$

This case delivers the minimum number of leaves and, therefore, the shortest experimental time, however the S/N ratio is also small. In the second case $\ln(\cos\alpha)$ dominates when $\alpha \to 90°$, but in this case the leaf-length $\to 0$, so the imaging readout becomes SPI. This case, surely, provides the highest possible S/N ratio, but requires impractically long experimental time and, therefore, is not considered further.

The most interesting third case occurs when both terms in the denominator of Eq. (5) make comparable contributions. In this case:

$$\cos\alpha = e^{-TR/T_1}, \tag{8}$$

which is the exact formula for the Ernst angle [11]. It should be noted that the derivation of the Ernst angle is based on the balance of small angle *RF*-excitation, which

reduces the magnetisation, and the magnetisation recovery between the *RF*-pulses. In the present case of Eq. (8), both terms are responsible for reduction of the magnetisation, and only their relative contribution is compared. Eq. (5) evolves into:

$$N < \frac{T_1}{2TR}, \tag{9}$$

and again an equation for the average leaf-length is

$$\text{Leaf-length} < \frac{T_1}{2}. \tag{10}$$

This case delivers an optimum S/N per unit of experimental time (see Appendix A) with the minimum contrast map blurring.

The minimum number of leaves for a certain imaging matrix can be derived from N:

$$\text{Number of leaves} > \frac{\text{number of } k\text{-space points}}{N}. \tag{11}$$

2.3. Parameter optimisation procedure

The optimisation procedure for TR, α and the number of leaves are investigated in this section. The discussion assumes that other imaging parameters have been selected in advance. The complete strategy, beyond the scope of this paper, can be found elsewhere [2,3].

The shortest possible TR is desirable, however T_2^* should be taken into consideration, in order to prevent possible distortion from residual transverse magnetisation, which is not fully de-phased before the next *RF* excitation. The lowest value of TR can also be limited by gradient rise time, which will not be considered here. So the first condition would be

$$TR \gtrsim T_2^*. \tag{12}$$

Two other parameters can be directly derived from TR. The excitation *RF*-pulse angle α follows from Eq. (8):

$$\alpha = \arccos(e^{-TR/T_1}). \tag{13}$$

The equation for the number of leaves is based on the total number of encoded k-space points, which depends on the selected type of trajectories. A detailed investigation of these issues can be found in [12]. Based on this number and Eq. (9), the optimum number of leaves would be

$$\text{Number of leaves} > \frac{\text{number of } k\text{-space points}}{T_1/2TR}. \tag{14}$$

2.4. Preparation sequences

Almost any bulk NMR pulse sequence may be used to generate image contrast with this approach. However, in order to demonstrate the principle, only T_1 (inversion recovery) and T_2 (spin–echo) preparations are presented in this paper.

2.4.1. Longitudinal relaxation time encoding

There are two main methods to perform T_1 encoding: saturation and inversion recovery and each methods has its pros and cons [11]. In this paper, we choose inversion recovery—the sequence requiring fewer *RF*-pulses. However, there are no known obstacles to the use of either as preparation for centric-scan SPRITE readout. The schematic sequence is displayed in Fig. 5a. Equilibrium magnetisation is inverted by the first 180° *RF*-pulse, then undergoes spin–lattice relaxation during the variable encoding time τ. Before the crusher the longitudinal magnetisation can be inverted once again, if necessary, by the pair of 90° *RF*-pulses, depicted by 90° + 90°. If the second inversion is not desired these pulses are used in opposite directions (90° – 90°), therefore the magnetisation undergos the same sequence of *RF*-pulse in both pathways of the phase cycle to remove recovering steady state magnetisation during imaging readout. The remaining transverse magnetisation is destroyed by the crasher gradient pulse. The stored magnetisation is read out by a SPRITE sequence.

2.4.2. Transverse relaxation time encoding

The T_2 preparation with the fewest *RF*-pulses is the spin–echo sequence, which is displayed in Fig. 5b. The initial magnetisation is rotated into the transverse plane and undergoes spin–spin relaxation, and the dispersion due to the localised magnetic field inhomogeneity is refocused by

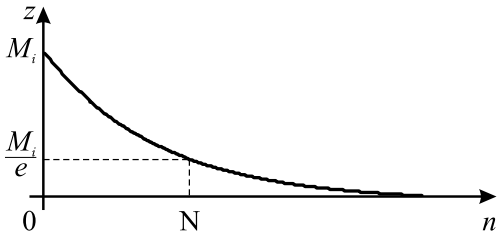

Fig. 4. The prepared magnetisation evolution during a centric-scan SPRITE readout. M_i, is the initial magnetisation, M_i/e, is the threshold level, at N, is the maximum number of points in each leaf.

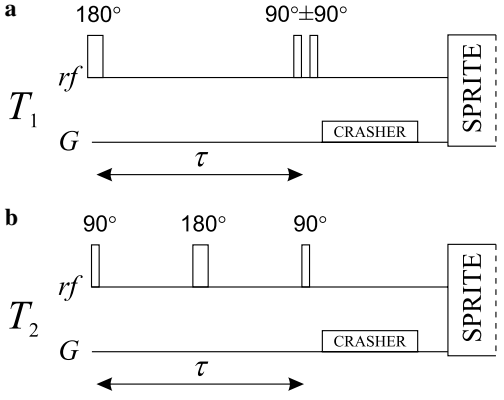

Fig. 5. The magnetisation preparation sequences with the SPRITE readout: (a) the inversion recovery sequence for T_1 encoding; (b) the spin–echo sequence for T_2 encoding.

a 180° *RF*-pulse. At the end of this procedure the magnetisation is stored along the longitudinal direction and the crasher gradient pulse is followed by a SPRITE readout.

3. Results and discussion

A thin cylindrical plastic container (invisible in MRI images) was used as a phantom (Fig. 6). The container was filled with 2 wt% agar gel, which was doped with 5.0 mM of $CuSO_4$ in order to reduce bulk lifetimes down to $T_1 = 140 \pm 10$ ms and $T_2 = 40 \pm 2$ ms. The sample has three cylindrical features, as shown in Fig. 6a. Two 9 mm diameter features (at the top) have the same proton density as the bulk sample, but different lifetimes: $T_1 = 80 \pm 10$ ms, $T_2 = 20 \pm 2$ ms. They are wrapped by teflon tape in order to prevent diffusional exchange with the bulk sample. The 10 mm diameter feature (at the bottom) has the same lifetimes as the bulk, but its thickness is reduced by 30%, which results in 30% less signal in 2D spin-density images without slice selection. The Fields of View were 40×40 mm with corresponding matrix dimensions of 64 points. All maps were constructed from 8 images, each with a different degree of contrast weighting [11]. All images were acquired with 16 averages. The sectoral trajectories with a specified number of leaves were used [12].

The following three sections are devoted to separate issues determining the quality of image derived NMR parameter maps. A summary section outlines a combined solution. In each section, the imaging parameters were chosen to highlight the issue under discussion. The first section investigates the edge enhancement effect, which can be noticeable when the imaging parameters are not chosen correctly. The second deals with the influence of *TR* on density and contrast maps. In the third, the upper limit of the number of leaves is investigated. And finally, selection of the most advantageous imaging parameters is introduced.

We note that in each of the three cases outlined below, in addition to all other experimental results reproduced in this paper, that our results are represented as maps of MR parameters of interest. Each map is derived from fitting a series of images where each image may be degraded by contrast weighting.

3.1. Edge enhancement effect

As mentioned in the theory section, the recovery of unprepared magnetisation plays a crucial role in contrast preparation mapping. Recovering magnetisation increases the signal at the outskirts of *k*-space to produce the edge enhancement effect. A typical edge-enhanced map is displayed in Fig. 7a, where a 1-leaf trajectory was used. The effect can be eliminated by moving from the asymptotic regime, where the influence of the steady state is great, to the pre-asymptotic regime, where the recovered magnetisation can still be neglected. This can be achieved by shortening the leaf-length, therefore increasing their number. A typical map of such a kind is displayed in Fig. 7b, where a 32-leaf trajectory was used. However, for quantitative contrast mapping the steady state has to be removed, which is achieved through the phase cycle of the storage *RF*-pulse. In this case, the number of leaves can be chosen arbitrarily. A T_1 map encoded by a 1-leaf trajectory, but with the steady state being removed, is shown in Fig. 7c. The edge enhancement effect is removed.

3.2. Image blurring: density versus contrast

When signal to noise is a limiting factor, a larger tip angle is unavoidable, which results in increased T_1-mediated blurring (Fig. 4, $M(k_{\max}) < M_i/e$). As examples, a density map (Fig. 8a) and a T_2 contrast map (Fig. 8d) are presented. These maps are encoded with a 1-leaf trajectory, $TR = 0.5$ ms and 10° excitation pulses. Extensive blurring can be observed on both maps. Increasing the repetition time (*TR*) elevates the steady state and therefore significantly reduces blurring of the density map (Fig. 8b). In the contrast map the steady state has been removed, and the change of *TR* produces the totally opposite effect (Fig. 8e and Eq. (4)), due to the prolonged evolution of the prepared magnetisation. A solution to the issue of blurring, for both density and contrast mapping, lies in the

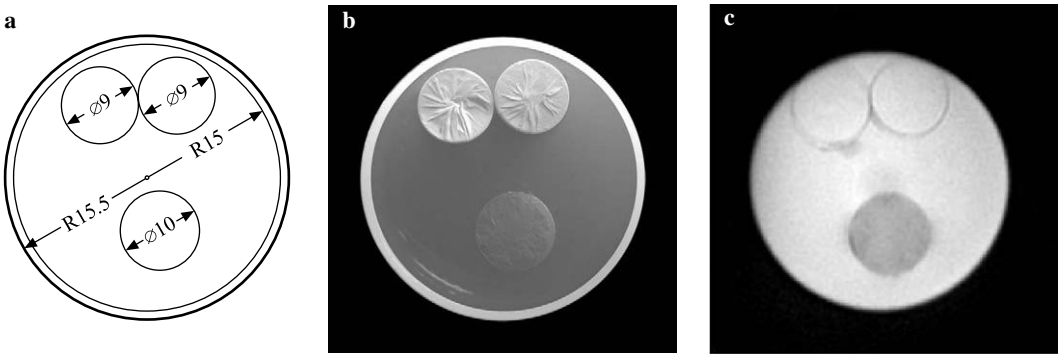

Fig. 6. A doped gel phantom: (a) sample scheme (all sizes are in mm); (b) photograph; (c) 2D SPRITE image. The ∅9 mm features have different lifetimes, and the ∅10 mm feature has different density (in 2D projection) compared to the bulk sample.

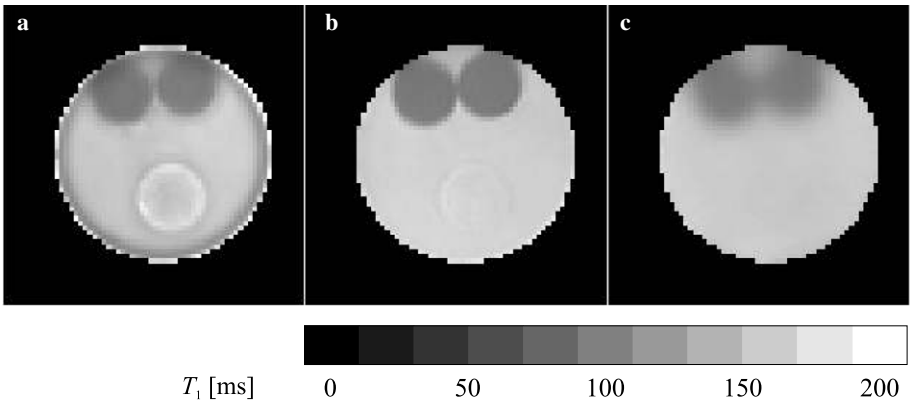

Fig. 7. An example of the Edge Enhancement artefact. 2D SPRITE T_1 maps: (a) 1-leaf trajectory, with the steady state, $t_{exp} \approx 5$ min; (b) 32-leaf trajectory, with the steady state, $t_{exp} \approx 50$ min; (c) 1-leaf trajectory, without steady state. Other parameters: $TR = 0.5$ ms, $\alpha = 2°$, $t_{exp} \approx 5$ min, number of scans, $ns = 16$.

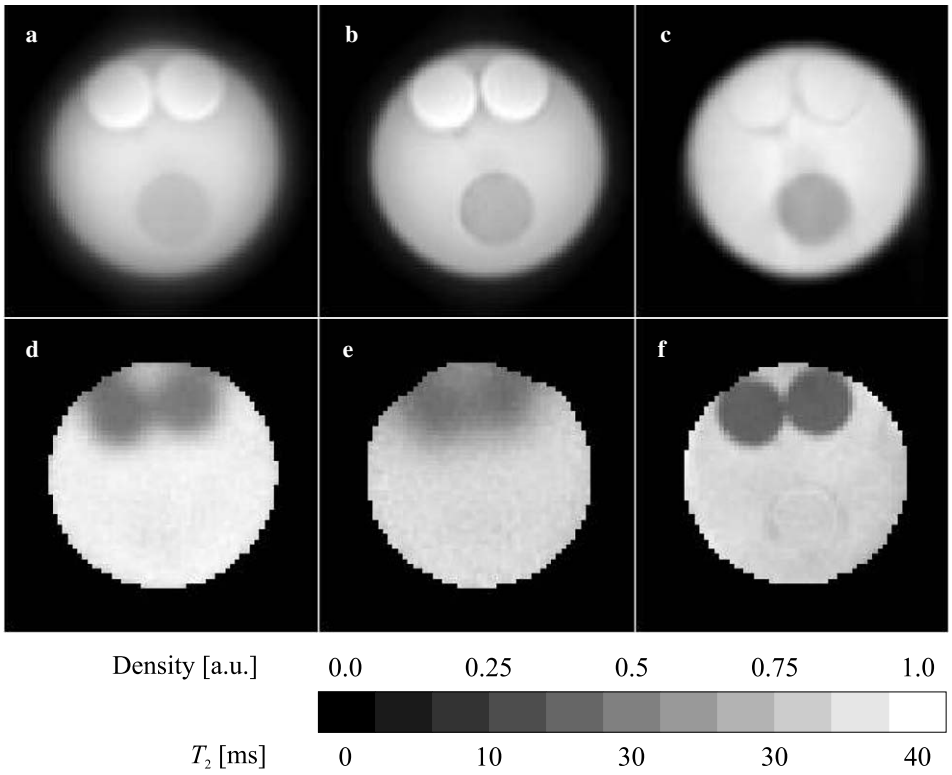

Fig. 8. Imaging and contrast resolution. 2D SPRITE density maps: (a) 1-leaf, $TR = 0.5$ ms, $t_{exp} \approx 40$ s; (b) 1-leaf, $TR = 2.5$ ms, $t_{exp} \approx 140$ s; (c) 32-leaf, $TR = 0.5$ ms, $t_{exp} \approx 6.5$ min. 2D SPRITE T_2 maps: (d) 1-leaf, $TR = 0.5$ ms, $t_{exp} \approx 5$ min; (e) 1-leaf, $TR = 2.5$ ms, $t_{exp} \approx 18.5$ min; (f) 32-leaf, $TR = 0.5$ ms, $t_{exp} \approx 50$ min. The tip angle was $\alpha = 10°$, $ns = 16$.

reduction of the leaf-length, and, in this case, true density (Fig. 8c) and contrast (Fig. 8f) maps are produced.

3.3. Number of leaves versus blurring

Since the large number of leaves increases the total experimental time, it is important to be able to find its optimal value. For small tip angles ($\alpha < \alpha_E = 4.5°$) the influence of the cosine logarithm is negligible, therefore the maximum leaf-length (Eq. (7)) is equal to the T_1 of the sample and the experimental time is shortest. The number of leaves can be approximately calculated from Eq. (11). The phantom $T_1 = 140$ ms makes the number of leaves $\approx$10 for the 64×64 matrix and the shortest $TR = 0.5$ ms. T_1 and T_2 maps of the phantom are presented in Fig. 9. Both 1-leaf maps (Figs. 9a and d) have extensive blurring, whereas already the 8-leaf maps (Figs. 9b and e) are significantly improved. The 64-leaf maps (Figs. 9c and f) require prolonged experimental time, but do not deliver a further reduction in contrast blurring. It should also be noticed that visibility of the density feature in the T_2 maps with higher leaf numbers (Fig. 9e and especially Fig. 9f) is due to slight variations of

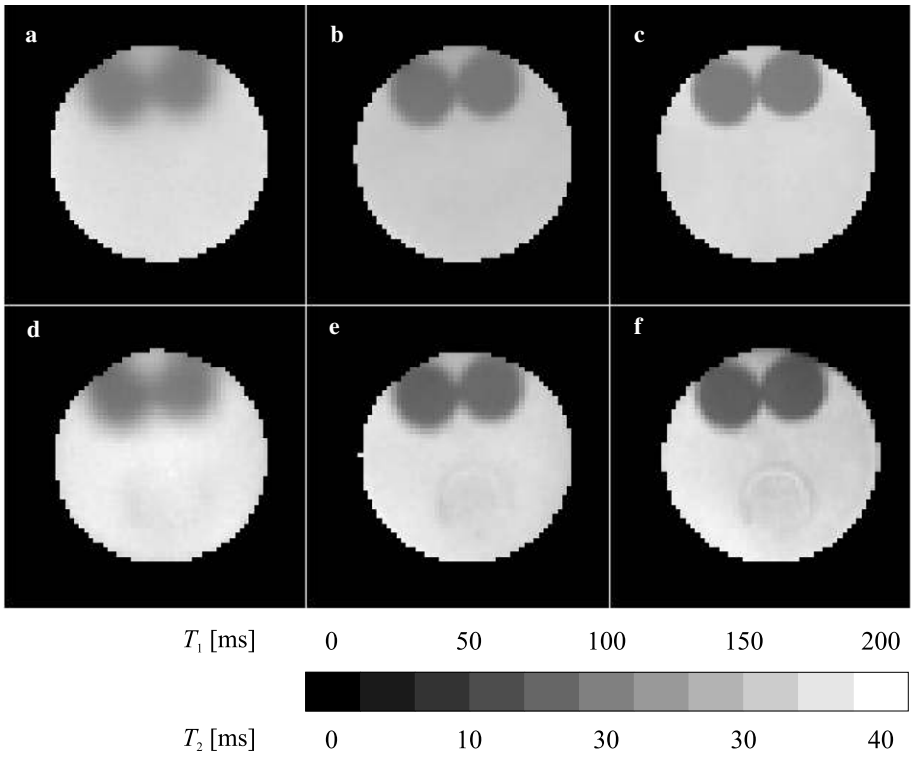

Fig. 9. The number of leaves vs resolution for maps obtained with $\alpha < \alpha_E$. 2D SPRITE T_1 maps: (a) 1-leaf, $t_{exp} \approx 40$ s; (b) 8-leaf, $t_{exp} \approx 115$ s; (c) 64-leaf, $t_{exp} \approx 12$ min. 2D SPRITE T_2 maps: (d) 1-leaf, $t_{exp} \approx 5$ min; (e) 8-leaf, $t_{exp} \approx 15$ min; (f) 64-leaf, $t_{exp} \approx 100$ min. Other parameters: $TR = 0.5$ ms, $\alpha = 2°$, $ns = 16$.

T_2^* around edges, which are imperfectly refocused by the spin–echo preparation sequence. This additional T_2^* contrast is probably caused by sample manufacture defects. The 1-leaf T_2 (Fig. 9d) map does not reveal these variations due to its severe blurring and the T_1 maps (Figs. 9a–c) are less sensitive to such T_2^* variations.

3.4. Measurement of a short T_2^* sample

A disk shaped *cis*-polybutadiene phantom with a variety of geometrical features was imaged as a short T_2^* example. The outer diameter of the MRI-visible part is 38 mm, the central hole is 6 mm. A SPRITE image of the phantom is presented in Fig. 10a. The bulk lifetimes of the material are $T_1 = 210 \pm 10$ ms, $T_2 = 560 \pm 20$ μs and $T_2^* = 330 \pm 10$ μs. All maps were acquired with an encoding time $t_p = 80$ μs. The Fields of View were 50×50 mm with a corresponding matrix dimension of 64 points. All maps were constructed from 8 images, each with a different degree of contrast weighting. All images were acquired with 16 averages. The sectoral 16-leaf trajectories were used [12].

The strategy presented in the theory section was used in order to calculate TR, α, and the number of leaves. The repetition time was $TR = 0.5$ ms, in accordance with

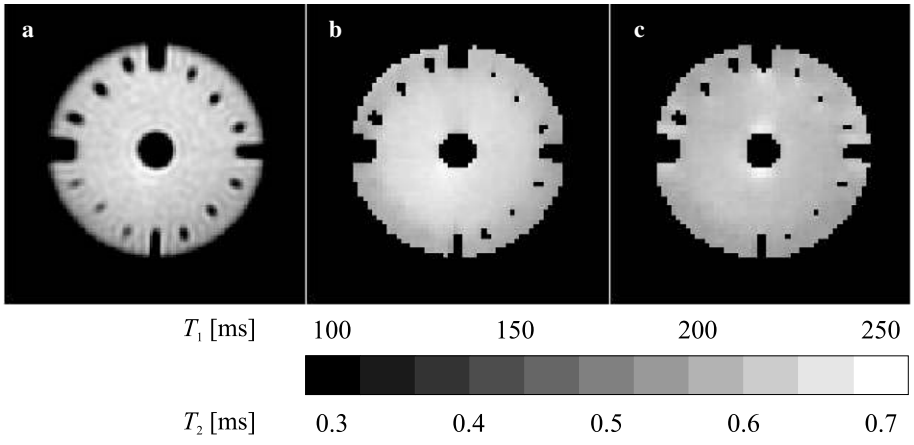

Fig. 10. A disk shaped *cis*-polybutadiene phantom. 2D SPRITE: (a) image, $t_{exp} \approx 5$ min; (b) T_1 map, $t_{exp} \approx 38$ min; (c) T_2 map, $t_{exp} \approx 38$ min. Imaging parameters: 16-leaf trajectory, $TR = 0.5$ ms, $\alpha = \alpha_E = 4°$, $ns = 16$.

Eq. (12). The tip angle of the excitation *RF*-pulses was $\alpha = 4°$ (see Eq. (13)), and the number of leaves was 16 (see Eq. (14)). T_1 and T_2 maps of the phantom are presented in Figs. 10b and c, respectively.

4. Conclusion

The SPRITE technique is well-suited to the generation of a variety of image contrasts by preparation of magnetisation prior to the imaging readout. This broadens the range of material structure and structural dynamics, which may be quantified by SPRITE in comparison with conventional MRI methods. This paper presents a detailed investigation of the contrast resolution, and introduces a strategy for selection of the most advantageous imaging parameters for the contrast mapping procedures. The rules may be summarised thus for the optimum case: the steady state magnetisation should be removed by phase cycling; tip angle $\alpha = \alpha_E$, the Ernst angle and the leaf-length should be $T_1/2$. This strategy is independent of the preparation sequence and can be readily adapted to 3D SPRITE and other low-tip-angle imaging methods, such as FLASH.

5. Experimental

The gel sample was made from granulated agar (Merck kGaA, Darmstadt, Germany) dissolved in distilled water.

All MRI measurements were performed on a MARAN spectrometer (Resonance Instrument Ltd., Oxford, United Kingdom) equipped with a 7T wide-bore, horizontal superconducting magnet 7T/60/AS (Magnex Scientific Ltd., Oxford, United Kingdom). A standard microimaging gradient set SGRAD156/100/S (Magnex Scientific Ltd., Oxford, United Kingdom) was used, powered by a set of three power amplifiers 7782 (AE Techron, Elkhart, USA), providing a maximum gradient strength of 0.36 T/m. A home-made 62 mm inner diameter probe was used with an *RF* power amplifier 7T100S (Communication Power Corp., New York, USA). All measurement were carried out at ambient temperature.

The Prospa (Magritek Ltd., Wellington, New Zealand) processing package was used for the data analysis and theoretical simulations.

All maps were prepared by thresholding pixel-by-pixel non-linear least squares fits of contrast weighted image data sets. The threshold was chosen individually for each case.

Acknowledgments

The authors thank B. MacMillan and R.P. MacGregor for their technical assistance and A. Marble for fruitful discussions. This work is partly supported by AFMnet, the Advanced Foods and Materials Network of Centres of Excellence. B.J.B. also thanks NSERC of Canada for Discovery and Equipment grants and the Canada Chairs program for a Research Chair in MRI of Materials (2002–2009). B.N. thanks NSERC of Canada for a Discovery grant. A.A.Kh is also thankful to F. Casanova and J. Perlo (RWTH-Aachen, Germany) for their valuable advice.

Appendix A

The optimisation of S/N per unit of experimental time is very often a complex task; a simplified case for a fixed *RF* tip angle, is presented here. In order to keep blurring below a certain limit, the maximum length of each leaf is limited (see Section 2). The main assumption in this analysis is that the leaf duration is shorter than the recovery time between leaves ($\approx 5T_1$) and can be neglected, therefore:

$$\text{Leaf-length} \ll 5T_1 \tag{15}$$

in the first instance, suppose that the solution satisfies this condition. In the case of short T_1 samples (some gases, porous media etc.) another approach is required. The total experimental time would be:

$$T_{\text{exp}} \approx 5T_1 \times \text{number of leaves}. \tag{16}$$

The number of leaves is known from Eq. (11), while N, the number of points per leaf, is taken from Eq. (5), therefore Eq. (16) evolves to:

$$\begin{aligned} T_{\text{exp}} &\approx 5T_1 \times N_k(TR/T_1 - \ln(\cos\alpha)) \\ &= 5N_k(TR - T_1\ln(\cos\alpha)), \end{aligned} \tag{17}$$

where N_k, is the number of sampled k-space points.

The S/N ratio for a single scan is:

$$S/N \propto \sin\alpha, \tag{18}$$

therefore, the formula for S/N per unit of experimental time would be

$$\frac{S/N}{T_{\text{exp}}} \propto \frac{\sin\alpha}{5N_k(TR - T_1\ln(\cos\alpha))}. \tag{19}$$

The corresponding graphs for a variety of T_1 values are shown in Fig. 11, where the y-axis is the S/N per unit of experimental time in arbitrary units and the x-axis is *RF*-pulse angle (α) normalised to the Ernst angle (α_E). The maximum can be found numerically and it occurs almost exactly where α is equal to the Ernst angle. For the purposes of this paper the discrepancy can be neglected.

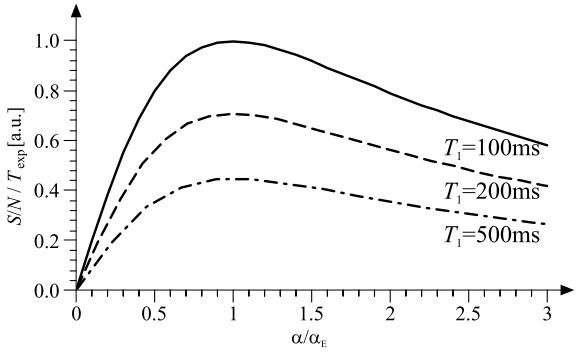

Fig. 11. S/N per unit of experimental time, where $TR = 0.5$ ms.

When $\alpha = \alpha_E$, the maximum leaf-length is less than $T_1/2$ (see Eq. (10)), therefore the condition of Eq. (15) is satisfied and our initial assumption is justified.

References

[1] B.J. Balcom, R.P. MacGregor, S.D. Beyea, D.P. Green, R.L. Armstrong, T.W. Bremmer, Single-Point ramped imaging with T_1 enhancement (SPRITE), J. Magn. Reson. A 123 (1996) 131.

[2] M. Halse, D.J. Goodyear, B. MacMillan, P. Szomolanyi, D. Matheson, B.J. Balcom, Centric scan SPRITE magnetic resonance imaging, J. Magn. Reson. 165 (2003) 219.

[3] M. Halse, J. Rioux, S. Romanzetti, J. Kaffanke, B. MacMillan, I. Mastikhin, N.J. Shah, E. Aubanel, B.J. Balcom, Centric scan SPRITE magnetic resonance imaging: optimization of SNR, resolution and relaxation time mapping, J. Magn. Reson. 169 (2004) 102.

[4] J. Hennig, A. Nauerth, H. Friedburg, RARE-imaging: a fast imaging method for clinical MR, Magn. Reson. Med. 3 (1986) 823.

[5] P. Mansfield, I.L. Pykett, Biological and Medical Imaging by NMR, J. Magn. Reson. 29 (1978) 355.

[6] A. Haase, J. Frahm, D. Matthei, W. Hänicke, K.D. Merboldt, FLASH imaging. Rapid NMR imaging using low flip-angle pulses, J. Magn. Reson. 67 (1986) 258.

[7] A. Haase, Snapshot FLASH MRI. Applications to T1, T2, and chemical-shift imaging, Magn. Reson. Med. 13 (1990) 77.

[8] I.V. Mastikhin, B.J. Balcom, P.J. Prado, C.B. Kennedy, SPRITE MRI with prepared magnetization and centric k space sampling, J. Magn. Reson. 136 (1999) 159.

[9] P.J. Prado, B.J. Balcom, I.V. Mastikhin, A.R. Cross, C.B. Kennedy, R.L. Armstrong, A. Logan, Magnetic resonance imaging of gases. A SPRITE study, J. Magn. Reson. 137 (1999) 324.

[10] M.T. Vlaardingerbroek, J.R. den Boer, Magnetic Resonance Imaging, Springer, New York, 1996.

[11] P.T. Callaghan, Principles of Nuclear Magnetic Resonance Microspcopy, Clarendon Press, Oxford, 1991.

[12] A.A. Khrapitchev, B. Newling, B.J. Balcom, Sectoral sampling in centric-scan SPRITE magnetic resonance imaging, J. Magn. Reson. 178 (2006) 288.